Global and Planetary Change 211 (2022) 103789

Contents lists available at ScienceDirect

Global and Planetary Change

journal homepage: www.elsevier.com/locate/gloplacha

Research article

Enhanced aridification across the Eocene/Oligocene transition evidenced by geochemical record in the Tajik Basin, Central Asia

Jimin Sun [a,b,*], Weiguo Liu [b,c], Zhengtang Guo [a,b], Liang Qi [b,d], Zhiliang Zhang [e]

[a] Key Laboratory of Cenozoic Geology and Environment, Institute of Geology and Geophysics, Chinese Academy of Sciences, Beijing 100029, China
[b] University of Chinese Academy of Sciences, Beijing 100049, China
[c] Institute of Earth Environment, Chinese Academy of Sciences, Xi'an 710061, China
[d] Institute of Geochemistry, Chinese Academy of Sciences, Guiyang 550081, China
[e] Institute of Geology, China Earthquake Administration, Beijing 100029, China

ARTICLE INFO

Editor: Dr. Liviu Matenco

Keywords:
Late Paleogene
Tajik Basin
Land-sea change
Stable isotope
Paleoenvironment

ABSTRACT

The Tajik Basin is an intermontane depression between the mountain ranges of Tian Shan, Pamir, and Hindu-kush, which is located in the northwestern part of the India-Asia collision zone. Due to the westward retreat of the Neotethys Sea, the paleoenvironment of the Tajik Basin has underwent change from a shallow-sea to a continental semiarid land during the Cenozoic era. This implies that the long-term climatic record in the Tajik Basin can potentially reflect the environmental effects of the changed land-sea distributions controlled by plate collision and global eustatic sea-level changes. In this paper, we present new results of stable oxygen and carbon isotopes of carbonates and chemical weathering indices of bulk samples from the Eocene-Oligocene terrestrial strata (ca. 39–30 Ma) in the center of the Tajik Basin. The temporal variations of oxygen and carbon isotopes of carbonates indicate an isotopic shift across the Eocene-Oligocene transition (~34 Ma), characterized by a relatively positive shift due to the isotopic enrichment in authigenic carbonates in an enhanced aridification episode in the Tajik Basin. This shift was also mirrored by the weakened chemical weathering indicated by the ratios of major oxides across the Eocene-Oligocene transition. Such a regional climatic shift was generally coincident with a remarkable global scale sea-level drop. We suggest that the isolated Paratethys Sea, which was mainly driven by global cooling due to the initial formation of the Antarctica Ice-sheet, together with the decreased seawater evaporation due to lower sea surface temperature, reduced water vapor transport by westerlies to the downwind region, and thus intensified the aridification in the Tajik Basin began at ~34 Ma.

1. Introduction

The Cenozoic era experienced a general climatic trend from warm to cool, which was superimposed by a series of dramatic climatic changes (Zachos et al., 2008). One of the most prominent climatic transition was at the Eocene–Oligocene Transition (EOT), marked by a climatic shift from a "greenhouse" to an "icehouse" world (Miller et al., 1987; Lear et al., 2000; Zachos et al., 2001; Liu et al., 2009). This event was firstly revealed by an isotope shift towards higher $\delta^{18}O$ values of deep-sea benthic foraminifera. Later application of planktonic foraminifera Mg/Ca palaeothermometry (Lear et al., 2008) and biomaker proxies of $U^{K'}_{37}$ and TEX_{86} (Liu et al., 2009) yielded a ~3 to 5 °C cooling in sea surface temperature across this climatic transition (Lear et al., 2008; Liu et al., 2009). Two main mechanisms have been proposed to interpret this greenhouse-to-icehouse transition including the opening of the Southern Ocean gateways, which led to the onset of the Antarctic Circumpolar Current and thus the thermal isolation of Antarctica (Kennett, 1977; Barker et al., 2007); and a decline in atmospheric pCO_2 and thus the formation of dynamic ice caps on high Antarctic plateau (DeConto and Pollard, 2003).

Except the numerous studies of the EOT event from the deep-sea drilling cores (e.g., Kennett, 1977; Zachos et al., 2001; Lear et al., 2008), this climatic transition was also investigated in East Asia. In the northeastern Tibetan Plateau, enhanced aridification across the EOT was recorded in the Xining Basin (Dupont-Nivet et al., 2007; Xiao et al., 2010; Hoorn et al., 2012; Zhang and Guo, 2014; Page et al., 2019), the Qaidam Basin (Ye et al., 2018; Sun et al., 2020a), and the Lanzhou Basin (Ao et al., 2020). In the inland basins in the northwestern China and

* Corresponding author at: Institute of Geology and Geophysics, Chinese Academy of Sciences, Beijing 100029, China.
E-mail address: jmsun@mail.iggcas.ac.cn (J. Sun).

https://doi.org/10.1016/j.gloplacha.2022.103789
Received 11 January 2022; Received in revised form 11 March 2022; Accepted 14 March 2022
Available online 18 March 2022

Mongolia, faunal records indicate a large mammal turnover at the EOT (Meng and McKenna, 1998; Kraatz and Geisler, 2010; Sun et al., 2014), and paleoclimatic studies suggest enhanced aridification marked by the transition to dry steppe (Sun and Windley, 2015) or steppe desert (Barbolini et al., 2020) across the EOT.

Although the climatic event across the EOT has been reported in East Asia, there still lacks a long-term climatic curve based on multiple climatic proxy indices in the Tajik Basin, Central Asia. Geological evidence indicates that there was once a large epicontinental sea (the proto-Paratethys Sea) extending from the Mediterranean Tethys in the west to the Tajik and Tarim Basins in the east, occupied an large area in Central Asia before ~39 Ma (Popov et al., 2004; Bosboom et al., 2014a, 2014b; Carrapa et al., 2015; Sun et al., 2016, 2020b; Bosboom et al., 2017; Kaya et al., 2019). However, this epicontinental sea underwent westward retreat driven by plate collision and global eustatic sea-level drop since the Eocene. The changes in land-sea distributions and the topographic changes must have affected moisture transport and aridification in the downwind inner Asia (e.g., Bosboom et al., 2014a; Carrapa et al., 2015; Wang et al., 2019; Sun et al., 2017, 2020b). Therefore, it is essential to understand the interplay between the retreat of the Paratethys and the regional aridification in Central Asia.

The objectives of this study aim to: (a) carry out new stable isotopes and chemical element analyses for the late Eocene-Oligocene strata in the Central Tajik Basin; b) reveal paleoclimatic changes across the Eocene-Oligocene transition; and (c) discuss the forcing mechanism of the long-term paleoclimatic changes in the Tajik Basin.

2. Geological settings

The Tajik Basin was once connected with the Tarim Basin before the northward indentation of the Pamirs, but now it is a structural depression constrained by the southwest Tian Shan (Gissar Range) to the north and the Pamirs to the east (Fig. 1a). These two mountains have experienced Cenozoic reactivation in response to the ongoing India-Asia collision (Burtman and Molnar, 1993; De Grave et al., 2012; Käßner et al., 2016). The Tajik Basin has received clastic materials reaching a thickness of up to 10 km (Thomas et al., 1994), consisting of Lower Jurassic to Quaternary strata. Sedimentological and detrital U—Pb age results suggest that Pamir mountains have been the primary source of sediments within the Tajik Basin as early as Cretaceous (Chapman et al., 2019) and Paleogene (Sun et al., 2020b), whereas the source materials from Tian Shan was much later until the late Miocene (Klocke et al., 2015).

As an intermontane basin, it is bounded by a series of large-scale faults defining this basin along the frontal mountain belts (Fig. 1a). The Mesozoic to Cenozoic strata have experienced tectonic shortening as an intracontinental deformation driven by the India-Eurasia collision, forming a series of north-south striking fold-and-thrust belts in the inner basin (Fig. 1a, b). These thrusts are doubly-vergent with opposite directions of dip. From the Pamirs to the central part of the basin, the thrusts are west-vergent, whereas they are east-vergent from the western to central part of the basin (Fig. 1b). The folds are fault-related asymmetry, thin-skinned anticlines, forming above a décollement level of

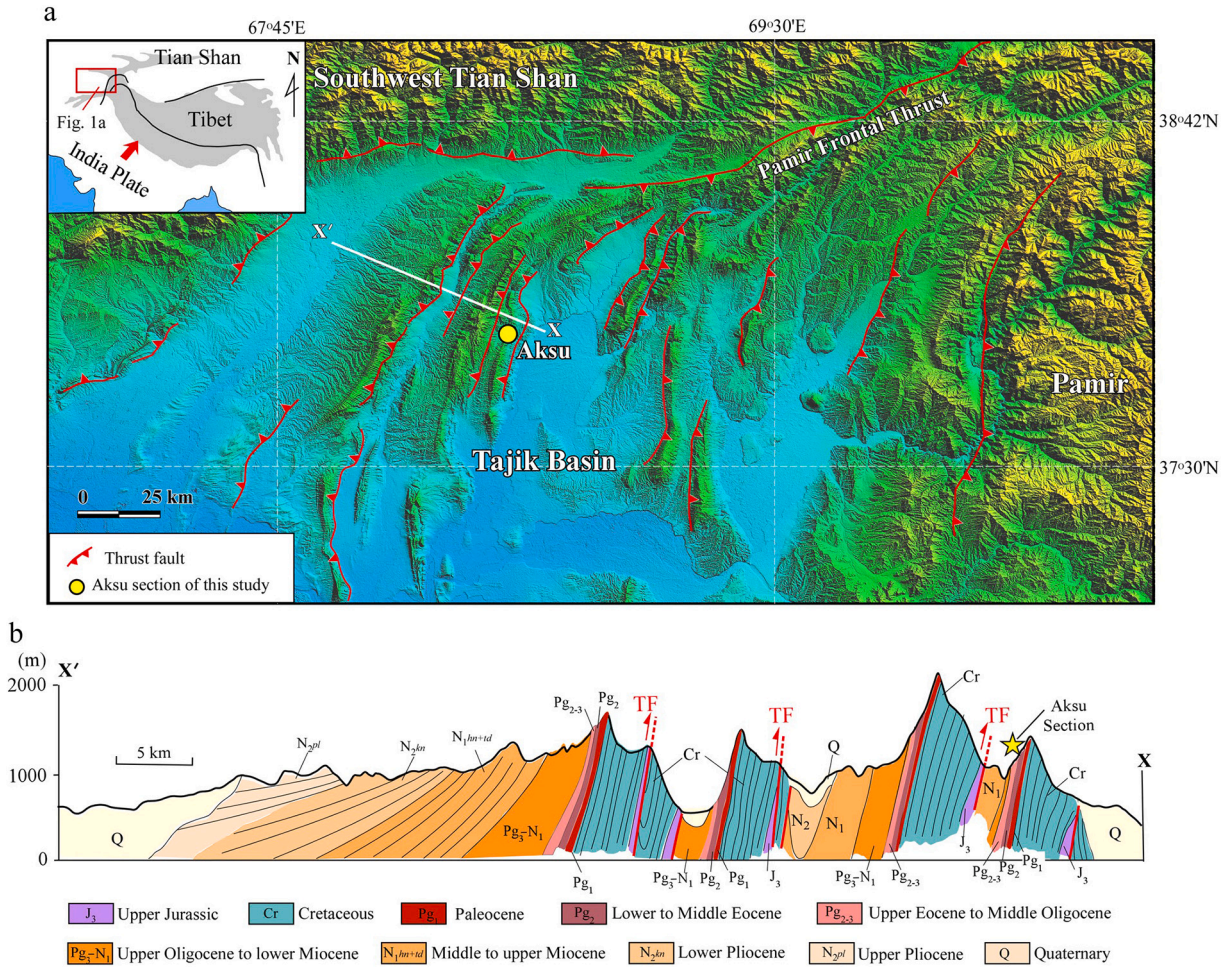

Fig. 1. (a) Digital Elevation Map shows the Tajik Basin and the adjoining mountains of Southwest Tian Shan and Pamir as well as the locations of the Aksu section and the section line of X-X′ of Fig. 1b; (b) Cross section shows thrusting and folding belts of the Mesozoic to Cenozoic strata within the Tajik Basin (modified from Zakharov, 1962). TF: Thrust fault.

Upper Jurassic evaporites (Fig. 1b) (Thomas et al., 1994).

Our section is located in the western limb of an asymmetry anticline cut by the Aksu river (from 38°06′33″N, 68°34′57″E, 817 m above sea level (asl) to 38°07′54″N, 68°34′50″E, 938 m asl) in the center of the Tajik Basin (Fig. 1a). This anticline is a fault-related fold which expose Cretaceous to Miocene strata in its western limb (Fig. 1b). Detrital apatite (U—Th)/He thermochronometry data of sandstone samples collected from the hanging wall of the thrust fault suggest that thrust induced exhumation and folding began at ca. 10–6 Ma (Lü et al., 2020).

The previous magnetostratigraphic chronology of the Aksu section focused on the well-exposed Upper Eocene to Lower Oligocene strata (Sun et al., 2020b). The lowest part of this section is marine deposits, consisting mainly of dark gray limestones, gray marlstones, and grayish green mudstones, but intercalated with thin-bedded gypsum and reddish brown mudstones (Fig. 2). Abundant marine bivalve fossils of *Cubitostrea plicata* (Solander) was discovered in the limestone. There is a remarkable boundary which defines the marine-terrestrial transition (Fig. 2a). The middle part of the section is characterized by the alternations of reddish brown siltstones and the interbedded sandstones (Fig. 2b), whereas the upper part is characterized by the occurrences of thin-bedded gypsum and gypsiferous mudstone (Fig. 2c) and the general alternations of brown sandstones and siltstones (Fig. 2d). The thickness of the studied section has a thickness of 1004 m, of which the lowest 200 m is marine sequence, while the remaining part is terrestrial deposition.

3. Materials and methods

In order to avoid the influences of the distinct depositional environments (marine and continental settings) on the interpretations of the climatic proxies, we only got fine-grained bulk samples from the terrestrial strata, of which 185 samples were collected for carbonate content and stable isotope analysis and 168 samples were taken for major element analysis. Detailed sampling positions are shown in Fig. 3.

3.1. Stable isotopic analysis of carbonates

Samples for $\delta^{18}O$ and $\delta^{13}C$ analyses of carbonates were analyzed using an isotope ratio mass spectrometer [MAT-252 (Finnigan)] with an automated carbonate preparation device (Kiel II) at the Institute of Earth Environment, Chinese Academy of Sciences, Xi'an, China. Oxygen and carbon isotope compositions are expressed in the delta (δ) notation relative to the V-PDB (Vienna-Pee Dee Belemnite) standard. Repeated analyses of laboratory carbonate standards with known $\delta^{18}O$ and $\delta^{13}C$ values indicate that the standard deviation is less than ±0.1‰.

3.2. Carbonate content analysis

Samples for carbonate content analyses were firstly grounded and sieved through a 100-mesh screen, and then approximately ~0.3 g material of each sample was analyzed for carbonate concentration by using the neutralization-titration method as described in detail by Liu et al. (2014). The analytical error of this method is about 0.5%.

3.3. Major element analysis

Samples were firstly grounded to 200-mesh. The major elements (except SiO_2) were measured by using ICP-OES (Agilent 720) with dilute factor of 1000 at the Institute of Geochemistry, Chinese Academy of

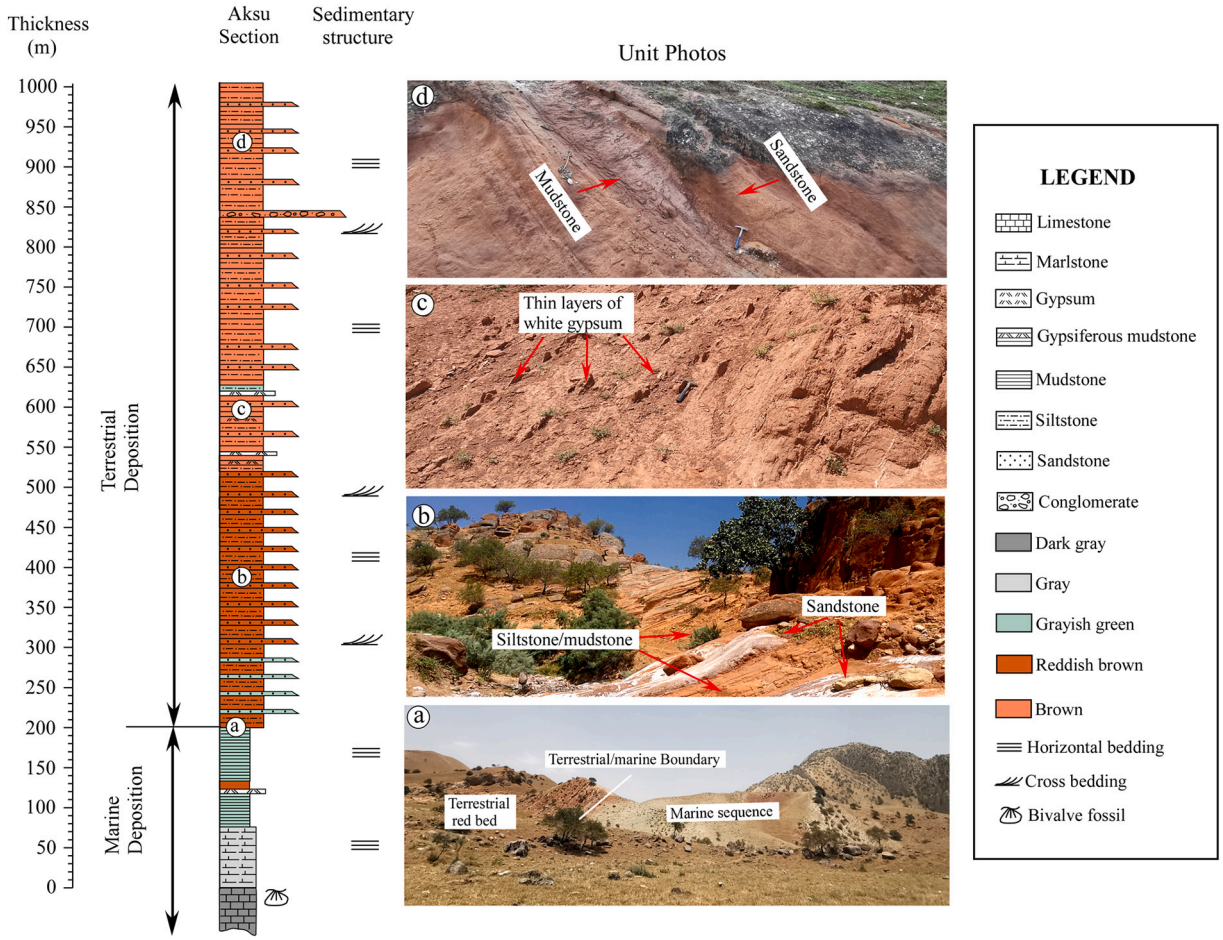

Fig. 2. Lithology, sedimentary structures, and the representative outcrops (a to d) in the Aksu section.

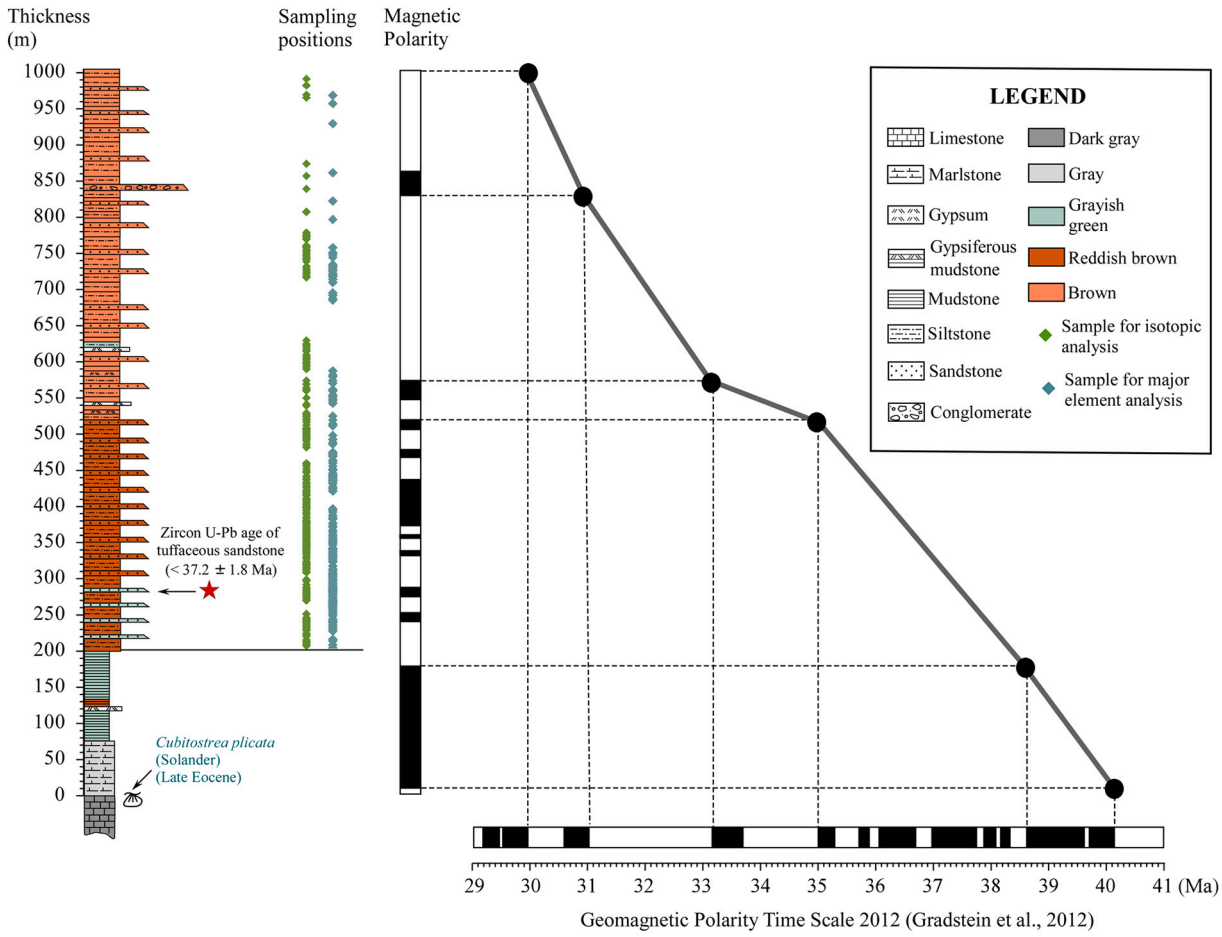

Fig. 3. Thickness vs. age plot of the Aksu section, the correlation was based on the magnetic polarity sequence, the zircon age of a tuffaceous sandstone, and the marine bivalve fossil age of this section (Sun et al., 2020b). Positions of samples are also shown.

Sciences. The sample preparation procedure is same as described in detail by Qi et al. (2000). The SiO_2 concentrations were measured using the technique of Alkali fusion. 0.05 g sample was dissolved with 0.25 g NaOH at 700 °C in Ag crucible for about 30 min. After cooling, the content was dissolved with hot water and acidified with 5 ml HCl and finally make up to 250 ml for ICP-OES measurement.

Sample for the loss on ignition (LOI) measurement (about 1 g for each sample) was weighed in porcelain crucible and heated at 900 °C in a muffle furnace for about 1 h, the weighted difference before and after the ignite is the LOI. It is necessary in calculating the concentrations of major oxides of samples.

The analytical accuracies are ±2% (relative) for major oxides in concentrations of greater than 0.5% and ± 5% (relative) for the others in concentrations of less than 0.5%.

3.4. Scanning electron microscope analysis

Thin-section from the fine-grained mudstone in the upper part of the section was examined for carbonate origin by using a Nova NanoSEM 450 field-emission scanning electron microscope (SEM) with 1 nm resolution, coupled with an Oxford Aztec energy dispersive X-ray spectrometers (EDS) at the Institute of Geology and Geophysics, Chinese Academy of Sciences. The SEM is used for microstructure analysis, while the Aztec EDS system is used for determining elements in or on the surface of minerals.

4. Results

The carbonate stable isotopes, together with the contents of carbonate and the ratios of major oxides were used to reconstruct paleoclimatic changes in the Tajik Basin. The magnetostratigraphy of this section was established by the correlation of the paleomagnetic polarity with the Geomagnetic Polarity Time Scale 2012 (GPTS 2012, Gradstein et al., 2012), which is based also on the other independent age constrains of the youngest U—Pb age of a tuffaceous sandstone and a late Eocene age of the marine fossil of *Cubitostrea plicata* (Solander) (Sun et al., 2020b) (Fig. 3). The magnetostratigraphy yields an age range from ~40.2 Ma to ~30 Ma, and the marine-terrestrial transition was at 38.6 Ma (Sun et al., 2020b). In order to have an age-dependent climatic reconstruction, linear interpolation between every two-neighboring paleomagnetic age tie-points in the plot of thickness versus GPTS 2012 was used to have corresponding ages for samples (Fig. 3).

4.1. Stable isotopes of carbonates

Stable isotopes of carbonates ($\delta^{18}O$ and $\delta^{13}C$) have been demonstrated to be powerful climatic parameters due to the isotope fractionations in lake evaporation or pedogenic processes (e.g., Talbot, 1990; Leng and Marshall, 2004). The temporal variations of the $\delta^{18}O$ and $\delta^{13}C$ are shown in Table A.1 and Fig. 4a, b, both of them show a remarkable change at around 34 Ma. From 38.6 to ~34 Ma, the $\delta^{18}O$ generally display more negative values with an average value of −9.7‰ (ranging from −11.6‰ to −8.4‰), but shifting to relatively positive values with a mean value of −8.6‰ (ranging from −10.4‰ to −6.2‰) after that time

(Fig. 4a). The difference between the $\delta^{18}O$ values before and after 34 Ma was significant based on the *t*-test, which is a statistic method to determine if there is a significant difference between the means of two data groups. The two-tailed t-test yields a *p* value (two-tailed) of 1.0×10^{-21}, which is much less than the critical *p* value of 0.05, suggesting that there is a significant difference. For the $\delta^{13}C$ record, more negative values are also in the strata of earlier than ~34 Ma with an average value of −2.3‰ (ranging from −7.0‰ to −0.5‰), whereas relatively positive values with a mean value of −1.0‰ (ranging from −2.9‰ to 0.8‰) after ~34 Ma (Fig. 4b). The two-tailed *t*-test result yields a *p* value of 3.4×10^{-11}, which is much less than the critical *p* value of 0.05, suggesting that the mean values of $\delta^{13}C$ are sufficient different before and after 34 Ma.

4.2. Carbonate content

The vertical variation of carbonate concentrations (Table A.1) generally shows a similar trend as those of the isotopes of $\delta^{18}O$ and $\delta^{13}C$ (Fig. 4c). The carbonate content had an average lower value of 13.3% (ranging from 5.1% to 24.8%) before 34 Ma, whereas it increased to 17.2% (ranging from 9.6% to 28%) after that time (Fig. 4c). The two-tailed t-test result yields a *p* value of 2.3×10^{-8} (less than the critical *p* value of 0.05), demonstrating that the mean values of carbonate contents are discernible before and after 34 Ma.

4.3. Major element ratios and the weathering indices

During the weathering process of sediments, the major elements have different geochemical behaviors characterized by diverse mobilization. Such features can be applied in examining the strength of chemical weathering (e.g., Nesbitt and Young, 1984; Fedo et al., 1995). Compared with the single element parameters, the major element ratios, which amplify the effects of chemical weathering, are more commonly used in inferring paleoclimatic changes (e.g., Guo et al., 1996; Retallack, 1999; Clift et al., 2008).

In the present study, all the ratios of major oxides (Table A.2) show a remarkable change at ~34 Ma (Fig. 5). The ratio of K_2O/Na_2O had higher values varying between 0.53 and 1.44 (mean value of 0.93) before ~34 Ma, while they had lower values ranging from 0.52 to 1.23 (mean value of 0.73) after that time (Fig. 5a). The ratio of SiO_2/Na_2O also shows similar variation trend as that of the K_2O/Na_2O (Fig. 5b), with a higher mean value of 52.4 (varying between 32.8 and 85.2)

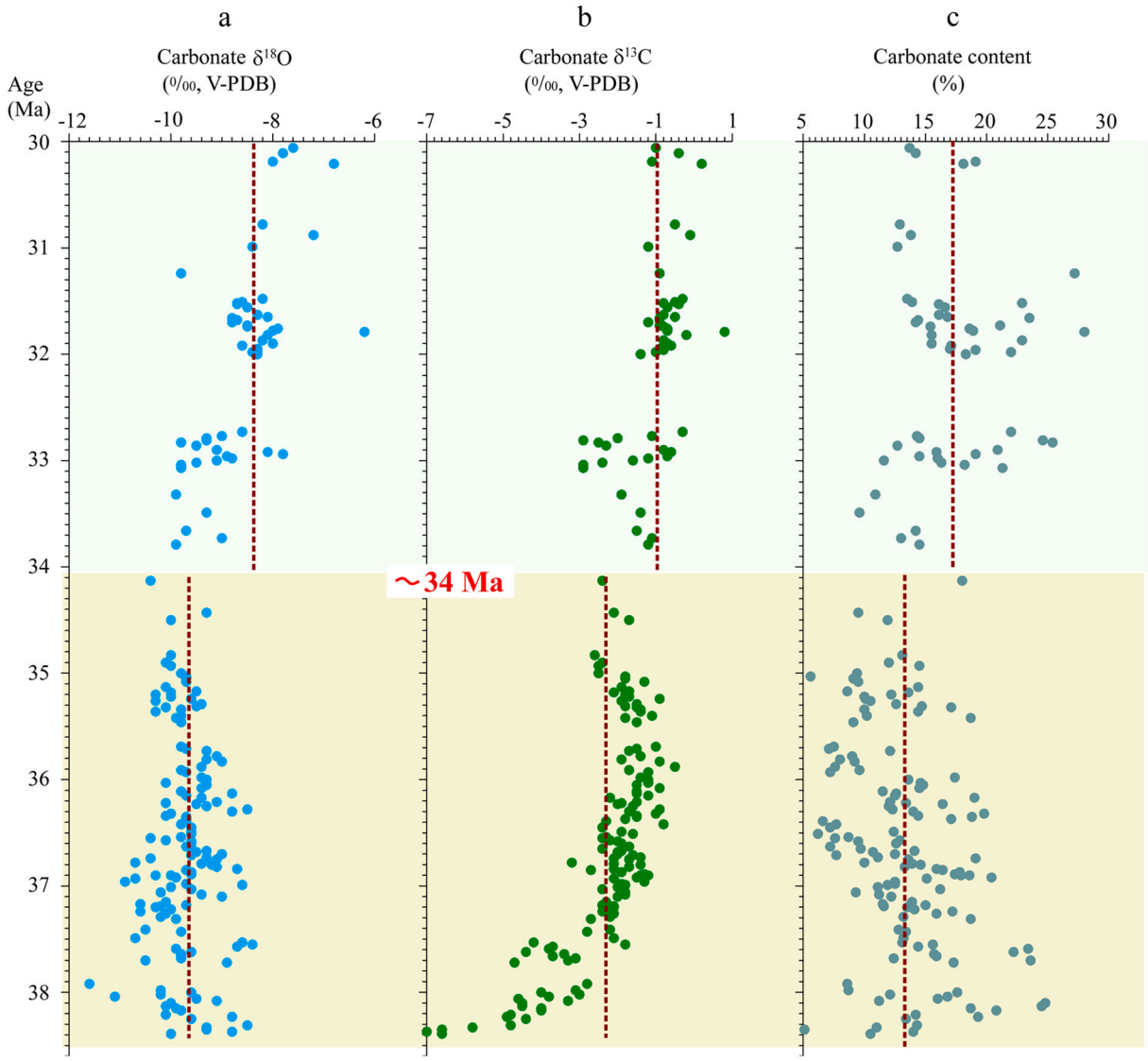

Fig. 4. Multiple climatic proxies of carbonates indicate paleoclimatic shift at ~34 Ma, (a) ^{18}O, (b) $\delta^{13}C$, and (c) carbonate content. The reddish dashed lines indicate the mean values of samples before and after ~34 Ma, respectively.

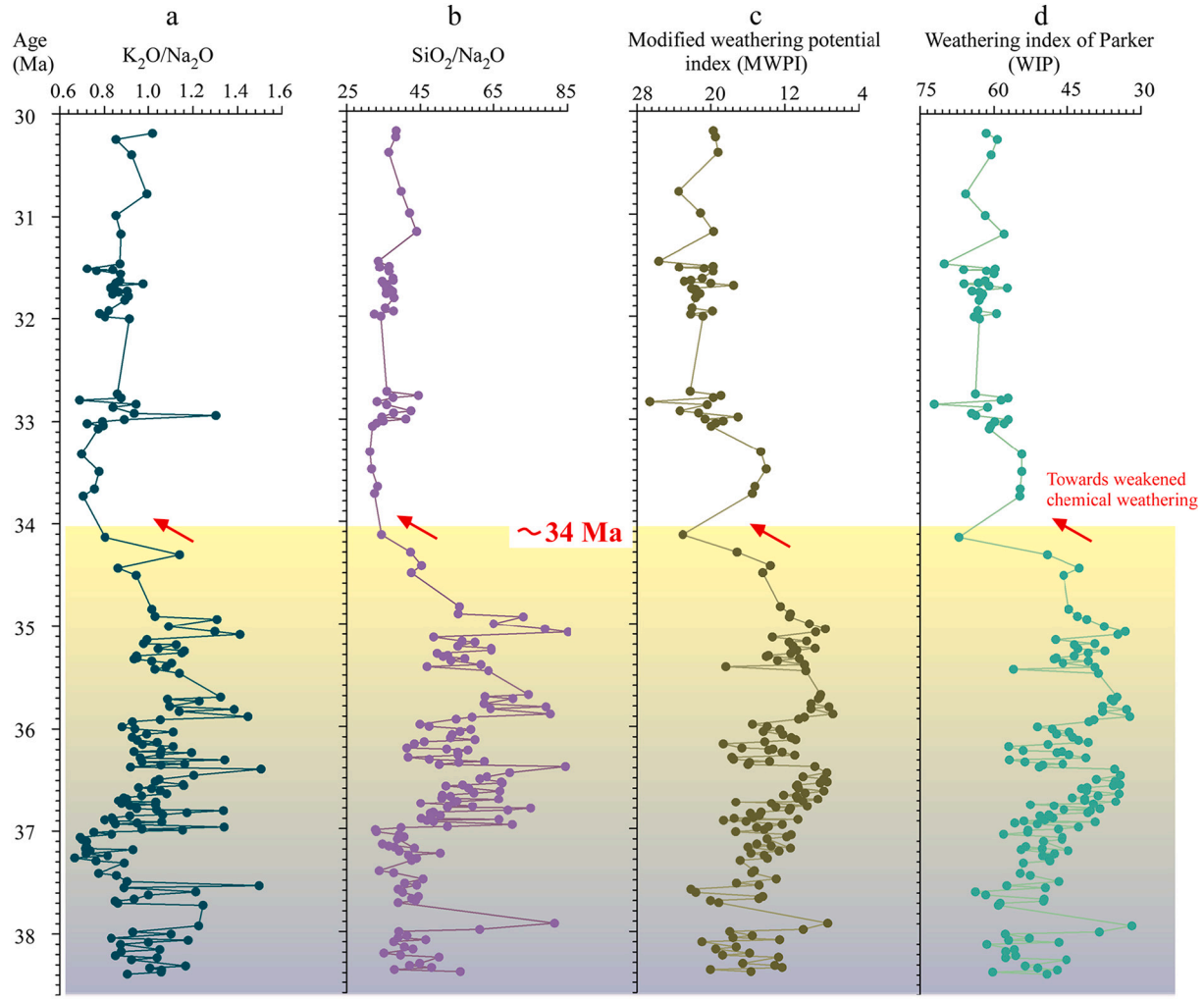

Fig. 5. Chemical weathering indices based on the ratios of major oxides indicate a remarkable paleoclimatic change at ~34 Ma, (a) K_2O/Na_2O, (b) SiO_2/Na_2O, (c) the modified weathering potential index (MWPI), and (d) the weathering index of Parker (WIP).

before ~34 Ma and a lower mean value of 36.3 (ranging from 31.3 to 44.4) after ~34 Ma. Different from the above simple ratios of oxides, some more complicated chemical indices are also used to infer paleoclimatic changes. Among them, the modified weathering potential index (MWPI), which was defined as the molecular ratio of $([(Na_2O + K_2O + CaO + MgO)/(Na_2O + K_2O + CaO + MgO + SiO_2 + A1_2O_3 + Fe_2O_3)] \times 100$ by Vogel (1975), and the weathering index of Parker (WIP, Parker, 1970), expressed as the molecular ratio of $[(2Na_2O/0.35) + (MgO/0.9) + (2K_2O/0.25) + (CaO/0.7)]$ x 100, are commonly used weathering indices. Both the chemical indices of MWPI and WIP show abrupt changes at ~34 Ma (Fig. 5c, d). Different from the variation trends of K_2O/Na_2O and SiO_2/Na_2O, MWPI and WIP had lower mean values of 13.3 (ranging from 6.8 to 23.0) and 46.4 (ranging from 31.9 to 63.8) before ~34 Ma and higher mean values of 20.4 (ranging from 14.0 to 26.6) and 61.3 (ranging from 54.3 to 72.1) after that time, respectively.

5. Discussions

The stable isotopes of carbonate and the major oxide ratios of the Aksu section were used to infer long-term paleoclimatic changes in the central Tajik Basin. Moreover, we also discussed the forcing mechanism of climatic changes related to the land-sea distributions and global changes.

5.1. Enhanced aridification across the Eocene-Oligocene transition indicated by stable isotopes of carbonates

Both the $\delta^{18}O$ and $\delta^{13}C$ records indicate a shift to relatively positive isotope values at ~34 Ma (Fig. 4a, b). We interpret this shift to enhanced aridification across the Eocene-Oligocene transition in the Tajik Basin. We have the following explanations: carbonates in sedimentary rocks commonly have two origins including detrital and authigenic carbonates. Different from the detrital carbonates which are - transported mainly by rivers to the - catchment, authigenic carbonates tend to be formed when lake hydrologic balance (between precipitation and evaporation) towards relatively direr conditions (e.g., Talbot and Kelts, 1986; Leng and Marshall, 2004; Horton et al., 2016), and such a process has a significant effect on the oxygen isotopic fraction of lake water and thus on the $\delta^{18}O$ of the authigenic carbonates. It has been demonstrated that in an inland lake system, the ^{16}O isotopes are preferentially lost during evaporation, leaving remaining lake water enriched in ^{18}O and thus resulting in relatively positive $\delta^{18}O$ of lake water (Leng and Marshall, 2004). Because the authigenic carbonates precipitated in lakes depends on the isotopic composition of lake water (Siegenthaler and Oeschger, 1980; Edwards and Wolfe, 1996), therefore the enhanced evaporation, can lead to the authigenic carbonate to be enriched in ^{18}O. In this context, the relatively positive $\delta^{18}O$ values after ~34 Ma were associated with more authigenic carbonates in an enhanced dry environment.

We have four lines of evidence to support this interpretation: (1) We found thin layers of gypsum and gypsiferous mudstones above the Eocene-Oligocene transition during the field investigation (Fig. 2c) (Sun et al., 2020b), they formed in ephemeral shallow lakes, water ponds or playas, which were developed on a floodplain due to periodic flooding of rivers when the hydrologic balance changed to relatively drier conditions; (2) In order to testify the existence of authigenic carbonates, we performed scanning electron microspore analysis of the thin section of the fine-grained mudstone interbedded in the strata above the Eocene-Oligocene transition. The SEM images show euhedral calcite crystals with lengths of 0.5–2 μm (Fig. 6a) suggesting an authigenic origin of such calcites, and their compositions are confirmed by energy spectrum analysis (Fig. 6b); (3) The temporal variations of carbonate content indicate that their concentrations were general higher after ~34 Ma (Fig. 4c), implying more authigenic carbonates under an hydrologic balance towards drier condition; and (4) The relationships between $\delta^{18}O$ and $\delta^{13}C$ of carbonates is often used to verify the degree of hydrological "closure" of lakes or water ponds through time (Talbot, 1990). Their correlations of the samples with two late Eocene age ranges (38.6 to 37.5 Ma; and 37.5 to 34.1 Ma), do not show any correlation between $\delta^{18}O$ and $\delta^{13}C$, evidenced by very low linear coefficient values of 0.24 and 0.30, respectively (Fig. 7a). The lack of covariance between $\delta^{18}O$ and $\delta^{13}C$ suggests that evaporation was not the main factor governing the isotopic composition of carbonates earlier than 34 Ma. In contrast, the $\delta^{18}O$ and $\delta^{13}C$ values shows a positive correlation, with a linear coefficient value of 0.79 (exceeding the threshold value of $\geq$0.7 for a strong positive correlation of closed lakes suggested by Talbot, 1990) (Fig. 7b), implying that the fine-grained lacustrine carbonates were formed in closed lakes and thus sensitively influenced by hydrological balance. Actually, it is very common for co-vary of $\delta^{18}O$ and $\delta^{13}C$ in closed basin lakes in arid zones (Leng and Marshall, 2004).

The much enhanced aridification can be also indicated by the relatively positive $\delta^{13}C$ values of carbonates after ~34 Ma (Fig. 4b). The $\delta^{13}C$ of authigenic carbonates in lake sediments mainly reflects the carbon isotope evolution of total dissolved inorganic carbon (TDIC) during the carbon cycle in the lake system (Paprocka, 2007). Generally, there are three predominant controls on the inorganic carbon isotope composition of the TDIC including the CO_2 exchange between atmosphere and lake water, the photosynthesis/respiration of aquatic plants within the lake (Vreča, 2003), and lake stratification and circulation (Myrbo and Shapley, 2006). However, both the aquatic biomass and the water-depth are very limited for ephemeral lakes or playas in arid regions, in such case, the most important factor that controls the $\delta^{13}C$ of the TDIC is the CO_2 exchange between atmosphere and lake water. There are two explanations for the relatively positive $\delta^{13}C$ values after ~34 Ma. Firstly, experimental and case studies in arid regions have confirmed that if lake hydrological balance towards drier climate, the intense evaporation will result in the preferentially removal of $^{12}CO_2$ from the dissolved inorganic carbon and thus enrich DIC ^{13}C of the remaining lake water (e.g., Li et al., 2012; Abongwa and Atekwana, 2013; Horton et al., 2016). Another potential factor is the effect of the decline atmospheric CO_2 contents on the isotopic equilibrium of carbon isotope. It has been demonstrated that the concentrations of atmospheric CO_2 fell from 1200 to 1000 ppm to 700 to 600 ppm across the Eocene/Oligocene transition (Pagani et al., 2011). The relatively lower partial pressure of atmospheric CO_2 after 34 Ma could lead to relative loss of $^{12}CO_2$ from lake water, resulting in enrichment in DIC ^{13}C in the remaining lake water.

5.2. *Enhanced aridification across the Eocene-Oligocene transition indicated by chemical weathering indices*

Weathering indices of ratios of major elements or their oxides are widely used in studying weathering degree of soil profiles (e.g., Nesbitt and Young, 1984; Fedo et al., 1995; Price and Velbel, 2003) and in paleoclimatic reconstructions (e.g., Guo et al., 1996; Retallack, 1999; Clift et al., 2008). During chemical weathering, some major elements tend to be preferentially lost as mobile elements (e.g., Na, Ca, Mg) (e.g., Nesbitt et al., 1980; Hamois, 1988). In contrast, some elements (Al, Si, Fe, Ti) are predominantly retained (e.g., Fedo et al., 1995; Babechuk et al., 2014). However, the weathering behavior of Fe is more complicated and dependent on the redox; trivalent (ferric) iron is relatively immobile, whereas divalent (ferrous) iron is highly mobile (Price and Velbel, 2003; Driese, 2004). Therefore, the weighted percentage of Fe_2O_3 increases with weathering intensity.

Although Na and K are both alkali elements, they have different geochemical behaviors. Na is the mobile element because it is readily leached during weathering. However, the geochemical behavior of K is much more complicated than Na. Although K may be mobile under strong chemical weathering, it can be also absorbed by clay minerals through ion exchange during weathering process (e.g., Hamois, 1988; Fedo et al., 1995), because the clay particles have a stronger tendency to adsorb and retain K^+ rather than Na^+ and Ca^{2+} due to the higher exchange capacity of K^+ (Kronberg et al., 1987). Case study also suggests that most Precambrian paleosols are enriched in K (Retallack, 1986). Therefore, the ratio of K_2O/Na_2O can be used as chemical weathering

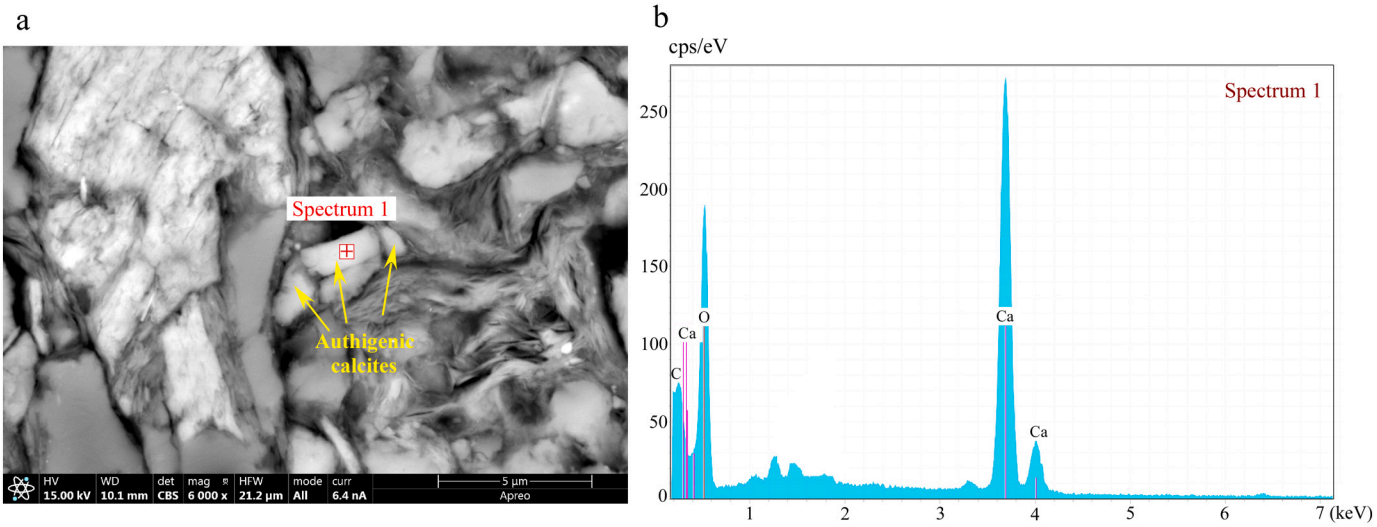

Fig. 6. (a) Scanning electron microscopy image of euhedral calcite crystals of authigenic origin; (b) the composition of calcite was confirmed by energy spectrum analysis.

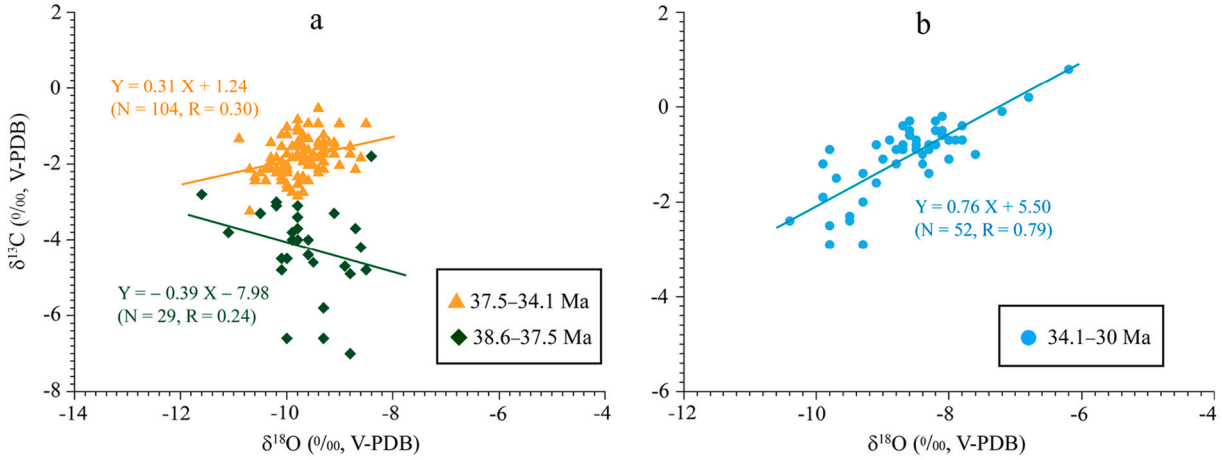

Fig. 7. Plots of $\delta^{18}O$ versus $\delta^{13}C$ of carbonates from the fine-grained terrestrial sediments of the Aksu section, showing the lacks of co-variations of the samples before ~34 Ma (from 38.6 to 37.5 Ma; 37.5 to 34.1 Ma) (a), and the linear positive covariance of them after ~34 Ma (b).

index, and the higher values imply stronger chemical weathering. The vertical variation trend of this ratio shows lower values after ~34 Ma (Fig. 5a), implying weakened chemical weathering and thus cold/dry climate after the Eocene-Oligocene transition, which is consistent with that of the stable isotope record of carbonates.

Si is also less leachable than Na (Parker, 1970; Babechuk et al., 2014), and the total proportion loss of Si is usually small during weathering (e.g., Parker, 1970). Therefore, the ratio of SiO_2/Na_2O can be also used as chemical weathering index, and the lower values of SiO_2/Na_2O after ~34 Ma also suggest weak chemical weathering (Fig. 5b), being comparable to the records indicated by the ratio of K_2O/Na_2O.

The modified weathering potential index of WMPI (Vogel, 1975), which defines the ratio of leachable bases relative to immobile oxides, has been used by many researchers as it considers most of the base oxides (Duzgoren-Aydin et al., 2002). Low MWPI values correspond to intense leaching of mobile oxides, thus implying strong chemical weathering; whereas high values imply less leaching of mobile oxides and thus weak chemical weathering. Fig. 5c shows that an abrupt shift of the MWPI occurred at ~34 Ma, which was marked by relatively higher values after ~34 Ma, this reflects the less leaching of the mobile oxides and thus weaker chemical weathering intensity after that time.

Additionally, the weathering index of WIP (Parker, 1970) is thought to be the most appropriate for inferring the weathering extent of both heterogeneous and homogeneous parent rocks (Price and Velbel, 2003). The WIP is based on the proportions of the alkali (Na, K) and alkaline (Ca, Mg) elements, which are the most mobile of the major elements. Another advantage of the WIP is that it takes into account the individual mobilities of sodium, potassium, magnesium and calcium, based on their bond strengths with oxygen (Parker, 1970). Although the WIP may not be used in strongly weathered profiles in humid tropical region where the alkali and alkaline elements may be totally leached (in this case, the WIP is zero), it is suitable for temperate climatic region. Because the WIP relies only on the mobile alkali and alkaline elements, the high value corresponds to weak chemical weathering and vice versa. The temporal variations of the WIP index show higher values and thus implying weaker chemical weathering and then the colder/drier climate after ~34 Ma (Fig. 5d).

We emphasized that we did not use the ratio of the Chemical Index of Alteration (CIA, Nesbitt and Young, 1982) because this index is mostly used for silicate rocks, especially for evaluating the extent of chemical weathering of feldspars (both plagioclase and k-feldspar) to clays (Nesbitt and Young, 1984; Fedo et al., 1995). The used content of CaO* in the CIA refers to the amount of CaO incorporated in the silicate fraction of rock (Nesbitt and Young, 1982), however, the samples of this study are reach in carbonates, which can be up to 28% (Fig. 4c), and it is difficult to actually determine the silicate-bound CaO (e.g., Buggle et al., 2011; Garzanti and Resentini, 2016), which may result in significant errors particularly for fluvial or marine sediments containing abundant carbonates (Garzanti and Resentini, 2016).

5.3. *Mechanisms for the enhanced aridification across the Eocene-Oligocene transition in the Tajik Basin*

To date, there have been different views about the time of the aridification in Central Asia, ranging from 40 Ma (Bosboom et al., 2014a), 39 Ma (Carrapa et al., 2015), 37–31 Ma (Bougeois et al., 2018; Wang et al., 2019), 34 Ma (Sun and Windley, 2015), Neogene (Kent-Corson et al., 2009), 25 Ma (Wang et al., 2020), 22 Ma (Guo et al., 2002), early Miocene (Graham et al., 2005), and to the middle-late Miocene (Ramstein et al., 1997).

Our new stable isotope records, together with the chemical weathering indices, indicate enhanced climatic aridification in the Tajik Basin at ~34 Ma just across the Eocene-Oligocene transition. It is interesting to discuss the forcing mechanism for this climatic shift with considerations of the potential roles of both the regional land-sea distributions and global climatic changes.

The regional climatic records of two representative parameters (Fig. 8a, b) were compared with the global sea-level fluctuations (Fig. 8c). This correlation suggests that the enhanced aridification and weakened chemical weathering across the Eocene-Oligocene transition in the Tajik Basin can be generally correlated with the prominent relative sea-level drop of up to 105 m reconstructed by the deep-sea isotopic record (e.g., Katz et al., 2008; Miller et al., 2020) (Fig. 8). Such a sea-level drop corresponds to a positive shift of $\delta^{18}O$ of the benthic foraminiferal *Cibicidoides* (Miller et al., 2020), implying the presence of large ice sheets (the Antarctic Ice-sheet) and development of an icehouse world in the beginning of the Oligocene (Miller and Fairbanks, 1985).

The sea-level drop of ~105 m would lead to a seawater retreat in the Neotethys, especially in its east part, where a large epicontinetal shallow-sea (proto-Paratethys) was once occupied in Central Asia (e.g., Popov et al., 2004). Although the magnetostratigraphic chronology of the Aksu section in the Central Tajik Basin (Sun et al., 2020b) and the U—Pb isotopic age of a volcanic tuff just above the marine-terrestrial transition in the northeastern Tajik Basin indicate seawater retreat at ca. 39 Ma (Carrapa et al., 2015), there still had a large shallow-sea to the west of the Tajik Basin (Fig. 9a). However, due to the large sea-level drop across the Eocene-Oligocene transition, together with the ongoing collision between the Indian continent with Asia as well as the Africa-Europe convergence (e.g., Rubatto et al., 1998; Rubatto and Hermann, 2001; Schulz et al., 2005), the previous widespread shallow

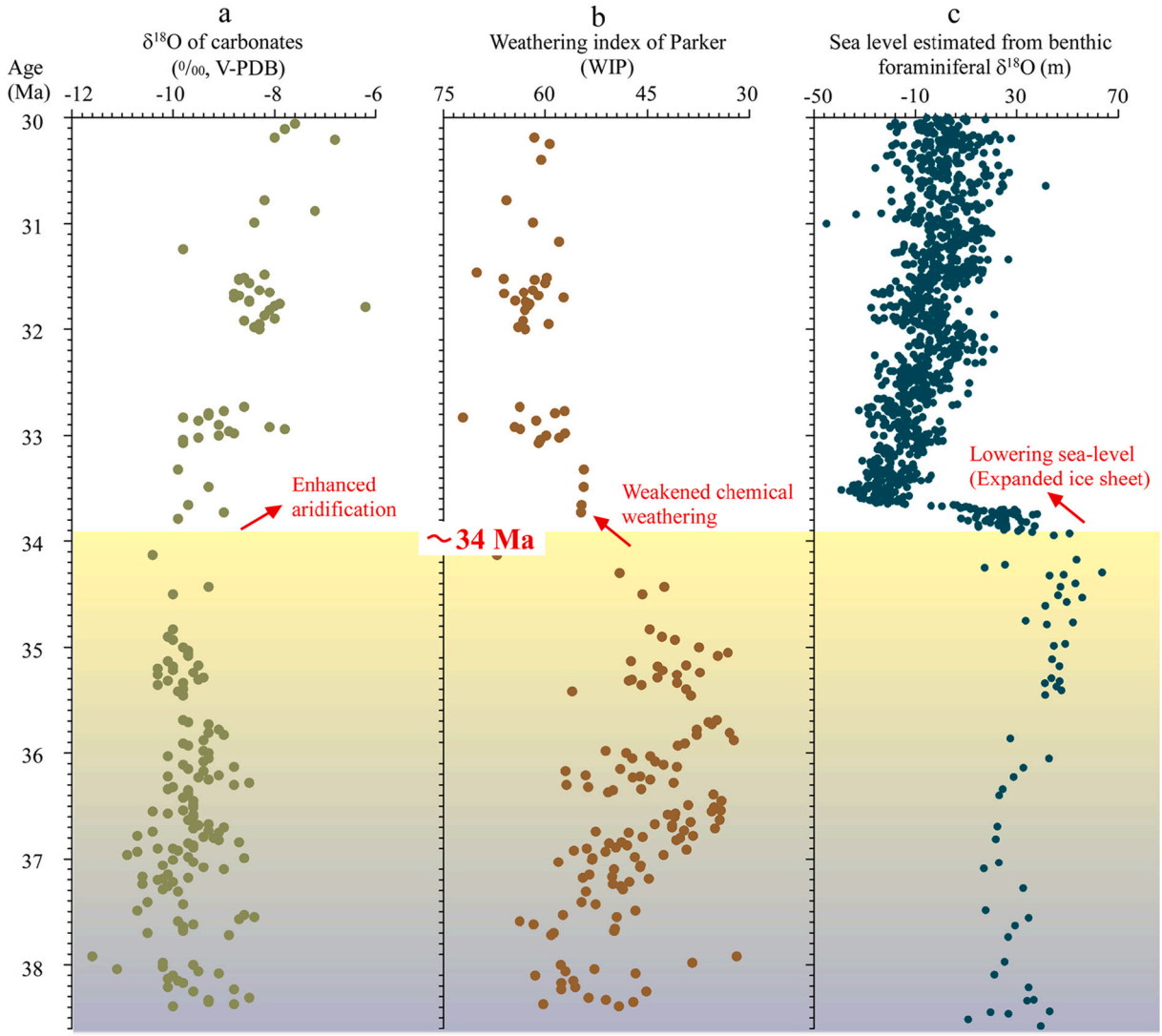

Fig. 8. The regional paleoclimatic changes as indicated by the $\delta^{18}O$ of carbonates and the chemical weathering index (WIP) can be generally correlated with the global sea-level fluctuations (data from Miller et al., 2020), noting the shifts around 34 Ma.

epicontinental sea experienced a remarkable regression, which led to a much contracted, nearly isolated Paratethys marginal sea occupied the inner Asian at about 34 Ma (Popov et al., 2004) (Fig. 9b). By that time, the closure of the Turgai Strait blocked the northern connection of the Paratethys with the West Siberian Sea (Popov et al., 2004); to the south it closed the connection with the Proto-Mediterranean Sea (Rögl, 1999; Popov et al., 2004; Schulz et al., 2005). There was only a possible narrow and shallow seaway restricted to its west (e.g., Rögl, 1999; Popov et al., 2004) (Fig. 9b). The birth of the isolated Paratethys as a marginal sea in the inner Asia at the Eocene-Oligocene boundary was also evidenced by the basin-side organic-rich sediments (hydrocarbon source rocks) and by the changing from diverse flora and fauna to monospecific species (e.g., Rögl, 1999; Schulz et al., 2005).

As we know, the climate of the Tajik Basin is dominated by the Westerlies (e.g., Caves et al., 2015; Heinecke et al., 2016; Prud'homme et al., 2021). The land-sea distributions in the Neotethys/Paratethys must have an important impact on the downwind Tajik Basin through modulating moisture transport by the Westerlies. The effect of retreated Paratethys seawater on the enhanced aridification in the Asian interior have been studied by case studies (e.g., Graham et al., 2005; Bosboom et al., 2014a; Carrapa et al., 2015; Caves et al., 2014, 2015; Sun and Windley, 2015; Bougeois et al., 2018; Meijer et al., 2019; Kaya et al., 2019) and by numerical modelling (e.g., Ramstein et al., 1997; Zhang et al., 2007; Li et al., 2018; Zhang et al., 2021). The modelling results demonstrate that westward seawater retreat influences the large-scale atmospheric circulation (Ramstein et al., 1997) and results in decreased precipitation in the inner Asia, driven by weakened water vapor transport from the ocean and an anomalous descending motion (Zhang et al., 2021). The modelling result highlights the major role of the Paratethys Sea as a thermal regulator of the Oligocene climate in Eurasia (e.g., Ramstein et al., 1997; Li et al., 2018).

On the other hand, both Mg/Ca ratios of planktonic foraminifera and biomarker proxies of marine records yielded a 3 to 5 °C cooling in the sea surface temperature (SST) since the beginning of the Oligocene (Lear et al., 2008; Liu et al., 2009), the decrease of SST would also reduce seawater evaporation and thus decrease the water vapor transportation from sea to continent.

In this context, in addition to the westward retreat of the Paratethys Sea, the deceased SST also played a minor role in reducing moisture transport from the west oceans to the inner Asia, resulting in much enhanced aridification began at ~34 Ma.

6. Conclusions

The inner Asian is now located in the largest mid-latitude arid zone in the northern Hemisphere. This region has experienced long-term

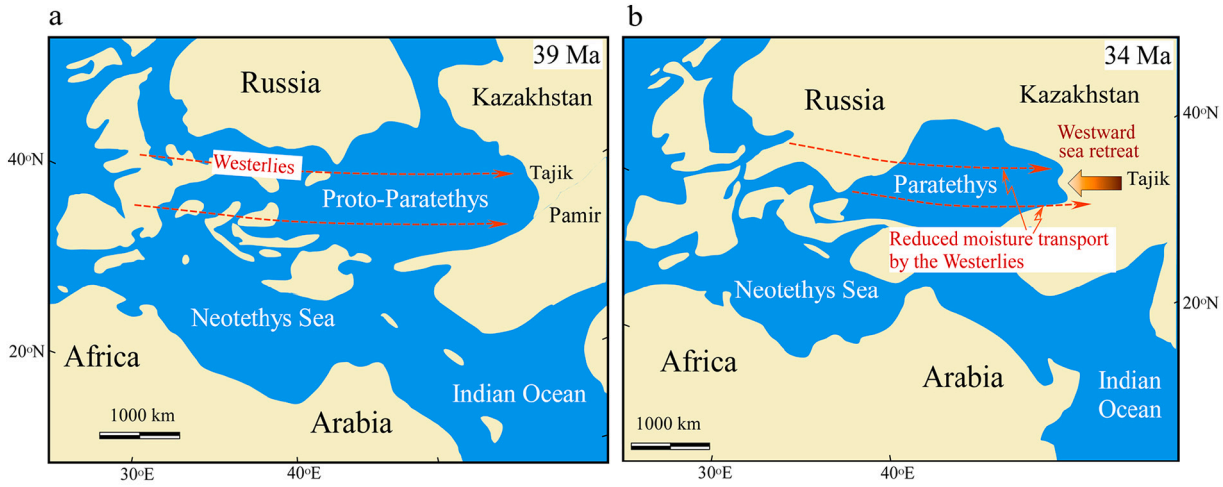

Fig. 9. Schematic maps show the effect of the land-sea distributions on the aridification in the Tajik Basin, Central Asia. (a) Palaeogeographic map shows the distributions of the Neotethys and the proto-Paratethys in the late Eocene (39 Ma) (modified from Popov et al., 2004, with consideration of the recent seawater retreat data of Carrapa et al. (2015) and Sun et al. (2020b) in the Tajik Basin); (b) the marine regression of the Proto-Paratethys (birth of the Paratethys from Popov et al., 2004) at ~34 Ma, together with the decreased seawater evaporation due to the lower sea-surface temperature, reduced moisture transport to the downwind Tajik Basin and led to the enhanced aridification since the beginning of the Oligocene.

stepwise aridification during the Cenozoic era, closely linked to the land-sea distributions, mountain building, and global climatic changes. The present study focuses on the paleoclimatic changes in central Tajik Basin during the late Paleogene, and we draw the following conclusions:

(1) Stable isotopes and chemical weathering indices were used to reconstruct paleoclimatic changes spanning the period from ~39 to 30 Ma in the Tajik Basin, they indicate enhanced aridification across the Eocene-Oligocene transition began at ~34 Ma.
(2) The regional climatic records can be generally correlated with the global sea-level fluctuations, characterized by the synchronous changes between the beginning of the intensified climatic aridification in the Tajik Basin and the remarkable global sea-level drop driven by the formation of the Antarctica Ice-sheet across the Eocene-Oligocene transition.
(3) The regression of the Neotethys Sea, marked by the birth of the isolated Paratethys marginal sea mainly in response to the global sea-level drop, together with the reduced seawater evaporation due to the decreased SST, diminished moisture transport by the Westerlies and led to the enhanced aridification that commenced ~34 Ma in the Tajik Basin.

Supplementary data to this article can be found online at https://doi.org/10.1016/j.gloplacha.2022.103789.

Declaration of Competing Interest

The authors declare that they have no competing financial interests or personal relationships that could have influenced the work reported in this paper.

Acknowledgements

This study was financially supported by the National Natural Science Foundation of China (41888101) and the Strategic Priority Research Program of Chinese Academy of Sciences (XDA20070202). The authors thank the two anonymous reviewers for their constructive comments, and thank Mustafo Gadoev and Sherzod Abdulov for their help in field sampling.

References

Abongwa, P.T., Atekwana, E.A., 2013. Assessing the temporal evolution of dissolved inorganic carbon in waters exposed to atmospheric $CO_{2(g)}$: a laboratory approach. J. Hydrol. 505, 250–265. https://doi.org/10.1016/j.jhydrol.2013.09.045.

Ao, H., Dupont-Nivet, G., Rohling, E.J., Zhang, P., Ladant, J.-B., Roberts, A.P., Licht, A., Liu, Q., Liu, Z., Dekkers, M.J., Coxall, H.K., Jin, Z., Huang, C., Xiao, G., Poulsen, C.J., Barbolini, N., Meijer, N., Sun, Q., Qiang, X., Yao, J., An, Z., 2020. Orbital climate variability on the northeastern Tibetan Plateau across the Eocene–Oligocene transition. Nat. Commun. 11, 5249. https://doi.org/10.1038/s41467-020-18824-8.

Babechuk, M.G., Widdowson, M., Kamber, B.S., 2014. Quantifying chemical weathering intensity and trace element release from two contrasting basalt profiles, Deccan Traps, India. Chem. Geol. 363, 56–75. https://doi.org/10.1016/j.chemgeo.2013.10.027.

Barbolini, N., Woutersen, A., Dupont-Nivet, G., Silvestro, D., Tardif, D., Coster, P.M.C., Meijer, N., Chang, C., Zhang, H., Licht, A., Rydin, C., Koutsodendris, A., Han, F., Rohrmann, A., Liu, X., Zhang, Y., Donnadieu, Y., Fluteau, F., Ladant, J.-B., Le Hir, G., Hoorn, C., 2020. Cenozoic evolution of the steppe-desert biome in Central Asia. Sci. Adv. 6 https://doi.org/10.1126/sciadv.abb8227 eabb8227.

Barker, P.F., Filippelli, G.M., Florindo, F., Martin, E.E., Scher, H.D., 2007. Onset and role of the Antarctic Circumpolar Current. Deep-Sea Res. II 54, 2388–2398.

Bosboom, R.E., Abels, H.A., Hoorn, C., van den Berg, B.C.J., Guo, Z., Dupont-Nivet, G., 2014a. Aridification in continental Asia after the Middle Eocene Climatic Optimum (MECO). Earth Planet. Sci. Lett. 389, 34–42. https://doi.org/10.1016/j.epsl.2013.12.014.

Bosboom, R.E., Dupont-Nivet, G., Grothe, A., Brinkhuis, H., Villa, G., Mandic, O., Stoica, M., Kouwenhoven, T., Huang, W., Yang, W., Guo, Z., 2014b. Timing, cause and impact of the late Eocene stepwise sea retreat from the Tarim Basin (West China). Palaeogeogr. Palaeoclimatol. Palaeoecol. 403, 101–118. https://doi.org/10.1016/j.palaeo.2014.03.035.

Bosboom, R., Mandic, O., Dupont-Nivet, G., Proust, J.N., Ormukov, C., Aminov, J., 2017. Late Eocene palaeogeography of the proto-Paratethys Sea in Central Asia (NW China, southern Kyrgyzstan and SW Tajikistan). Geol. Soc. London Spec. Publ. 427, 565–588. https://doi.org/10.1144/SP427.11.

Bougeois, L., Dupont-Nivet, G., de Rafélis, M., Tindall, J.C., Proust, J.-N., Reichart, G.-J., de Nooijer, L.J., Guo, Z., Ormukov, C., 2018. Asian monsoons and aridification response to Paleogene sea retreat and Neogene westerly shielding indicated by seasonality in Paratethys oysters. Earth Planet. Sci. Lett. 485, 99–110. https://doi.org/10.1016/j.epsl.2017.12.036.

Buggle, B., Glaser, B., Hambach, U., Gerasimenko, N., Markovic, S., 2011. An evaluation of geochemical weathering indices in loess-paleosol studies. Quat. Int. 240, 12–21. https://doi.org/10.1016/j.quaint.2010.07.019.

Burtman, V.S., Molnar, P., 1993. Geological and geophysical evidence for deep subduction of continental crust beneath the Pamir. Geol. Soc. Am. Spec. Pap. 281, 1–76.

Carrapa, B., DeCelles, P.G., Wang, X., Clementz, M.T., Mancin, N., Stoica, M., Kraatz, B., Meng, J., Abdulov, S., Chen, F.H., 2015. Tectono-climatic implications of Eocene Paratethys regression in the Tajik basin of central Asia. Earth Planet. Sci. Lett. 424, 168–178. https://doi.org/10.1016/j.epsl.2015.05.034.

Caves, J.K., Sjostrom, D.J., Mix, H.T., Winnick, M.J., Chamberlain, C.P., 2014. Aridification of Central Asia and uplift of the Altai and Hangay Mountains, Mongolia: Stable isotope evidence. Am. J. Sci. 314, 1171–1201. https://doi.org/10.2475/08.2014.01.

Caves, J.K., Winnick, M.J., Graham, S.A., Sjostrom, D.J., Mulch, A., Chamberlain, C.P., 2015. Role of the westerlies in Central Asia climate over the Cenozoic. Earth Planet. Sci. Lett. 428, 33–43. https://doi.org/10.1016/j.epsl.2015.07.023.

Chapman, J.B., Carrapa, B., DeCelles, P.G., Worthington, J., Mancin, N., Cobianchi, M., Stoica, M., Wang, X., Gadoev, M., Oimahmadov, I., 2019. The Tajik Basin: a composite record of sedimentary basin evolution in response to tectonics in the Pamir. Basin Res. 1–21. https://doi.org/10.1111/bre.12381.

Clift, P.D., Hodges, K.V., Heslop, D., Hannigan, R., Long, H.V., Clves, G., 2008. Correlation of Himalayan exhumation rates and Asian monsoon intensity. Nat. Geosci. 1, 875–880.

De Grave, J., Glorie, S., Ryabinin, A., Zhimulev, F., Buslov, M.M., Izmer, A., Elburg, M., Vanhaecke, F., Van den Haute, P., 2012. Late Palaeozoic and Meso-Cenozoic tectonic evolution of the southern Kyrgyz Tien Shan: Constraints from multi-method thermochronology in the Trans-Alai, Turkestan-Alai segment and the southeastern Ferghana Basin. J. Asian Earth Sci. 44, 149–168. https://doi.org/10.1016/j.jseaes.2011.04.019.

DeConto, R.M., Pollard, D., 2003. Rapid Cenozoic glaciation of Antarctica induced by declining atmospheric CO_2. Nature 421, 245–249.

Driese, S.G., 2004. Pedogenic translocation of Fe in modern and ancient vertisols and implications for interpretations of the Hekpoort paleosol (2.25 Ga). J. Geol. 112, 543–560.

Dupont-Nivet, G., Krijgsman, W., Langereis, C.G., Abels, H.A., Dai, S., Fang, X., 2007. Tibetan Plateau aridification linked to global cooling the Eocene–Oligocene transition. Nature 445, 635–638.

Duzgoren-Aydin, N.S., Aydin, A., Malpas, J., 2002. Re-assessment of chemical weathering indices: case study of pyroclastic rocks of Hong Kong. Eng. Geol. 63, 99–119.

Edwards, T.W.D., Wolfe, B.B., 1996. Influence of changing atmospheric circulation on precipitation $\delta^{18}O$-temperature relations in Canada during the Holocene. Quat. Res. 46, 211–218.

Fedo, C.M., Nesbitt, H.W., Young, G.M., 1995. Unraveling the effects of potassium metasomatism in sedimentary rocks and paleosols, with implications for paleoweathering conditions and provenance. Geology 23, 921–924.

Garzanti, E., Resentini, A., 2016. Provenance control on chemical indices of weathering (Taiwan river sands). Sediment. Geol. 336, 81–95. https://doi.org/10.1016/j.sedgeo.2015.06.013.

Gradstein, F.M., Ogg, J.G., Schmitz, M., Ogg, G., 2012. The Geologic Time Scale 2012. Cambridge University Press, Cambridge.

Graham, S.A., Chamberlain, C.P., Yue, Y., Ritts, B.D., Hanson, A.D., Horton, T.W., Waldbauer, J.R., Poage, M.A., Feng, X., 2005. Stable isotope records of Cenozoic climate and topography, Tibetan plateau and Tarim basin. Am. J. Sci. 305, 101–118. https://doi.org/10.2475/ajs.305.2.101.

Guo, Z.T., Liu, T.S., Guiot, J., Wu, N.Q., Lü, H.Y., Han, J.M., Liu, J.Q., Gu, Z.Y., 1996. High frequency pulses of East Asian monsoon climate in the last two glaciations: link with the North Atlantic. Clim. Dyn. 12, 701–709.

Guo, Z.T., Ruddiman, W.F., Hao, H.Z., Wu, H.B., Qiao, Y.S., Zhu, R.X., Peng, S.Z., Wei, J. J., Yuan, B.Y., Liu, T.S., 2002. Onset of Asian desertification by 22 Myr ago inferred from loess deposits in China. Nature 416, 159–163.

Hamois, L., 1988. The CIW index: A new chemical index of weathering. Sediment. Geol. 55, 319–322.

Heinecke, L., Mischke, S., Adler, K., Barth, A., Biskaborn, B.K., Plessen, B., Nitze, I., Kuhn, G., Rajabov, I., Herzschuh, U., 2016. Late Pleistocene to Holocene climate and limnological changes at Lake Karakul (Pamir Mountains, Tajikistan). Clim. Past Discuss. https://doi.org/10.5194/cp-2016-34.

Hoorn, C., Straathof, J., Abels, H.A., Xu, Y., Utescher, T., Dupont-Nivet, G., 2012. A late Eocene palynological record of climate change and Tibetan Plateau uplift (Xining Basin, China). Palaeogeogr. Palaeoclimatol. Palaeoecol. 344–345, 16–38. https://doi.org/10.1016/j.palaeo.2012.05.011.

Horton, T.W., Defliese, W.F., Tripati, A.K., Oze, C., 2016. Evaporation induced ^{18}O and ^{13}C enrichment in lake systems: a global perspective on hydrologic balance effects. Quat. Sci. Rev. 131, 365–379. https://doi.org/10.1016/j.quascirev.2015.06.030.

Käßner, A., Ratschbacher, L., Jonckheere, R., Enkelmann, E., Khan, J., Sonntag, B.-L., Gloaguen, R., Gadoev, M., Oimahmadov, I., 2016. Cenozoic intracontinental deformation and exhumation at the northwestern tip of the India-Asia collision—southwestern Tian Shan, Tajikistan, and Kyrgyzstan. Tectonics 35, 2171–2194. https://doi.org/10.1002/2015TC003897.

Katz, M.E., Miller, K.G., Wright, J.D., Wade, B.S., Browning, J.V., Cramer, B.S., Rosenthal, Y., 2008. Stepwise transition from the Eocene greenhouse to the Oligocene icehouse. Nat. Geosci. 1, 329–334.

Kaya, M.Y., Dupont-Nivet, G., Proust, J.N., Roperch, P., Bougeois, L., Meijer, N., Frieling, J., Fioroni, C., Altıner, S.Ö., Vardar, E., Barbolini, N., Stoica, M., Aminov, J., Mamtimin, M., Guo, Z., 2019. Paleogene evolution and demise of the proto-Paratethys Sea in Central Asia (Tarim and Tajik basins): role of intensified tectonic activity at ca. 41 Ma. Basin Res. 31, 461–486. https://doi.org/10.1111/bre.12330.

Kennett, J.P., 1977. Cenozoic evolution of Antarctic glaciation, the circum-Antarctic Ocean, and their impact on global paleoceanography. J. Geophys. Res. 82, 3843–3860.

Kent-Corson, M.L., Ritts, B.D., Zhuang, G., Bovet, P.M., Graham, S.A., Page Chamberlain, C., 2009. Stable isotopic constraints on the tectonic, topographic, and climatic evolution of the northern margin of the Tibetan Plateau. Earth Planet. Sci. Lett. 282, 158–166.

Klocke, M., Voigt, T., Kley, J., Pfeifer, S., Rocktäschel, T., Keil, S., Gaupp, R., 2015. Cenozoic evolution of the Pamir and Tien Shan mountains reflected in syntectonic deposits of the Tajik Basin. In: Brunet, M.-F., McCann, T., Sobel, E.R. (Eds.), Geological Evolution of Central Asian Basins and the Western Tien Shan Range, Geol. Soc. Spec. Publ., 427, pp. 523–564. https://doi.org/10.1144/SP427.7.

Kraatz, B.P., Geisler, J.H., 2010. Eocene–Oligocene transition in Central Asia and its effects on mammalian evolution. Geology 38, 111–114. https://doi.org/10.1130/G30619.1.

Kronberg, K.I., Nesbitt, H.W., Fyfe, W.S., 1987. Mobilities of alkalis, alkaline earths and halogens during weathering. Chem. Geol. 60, 41–49. https://doi.org/10.1016/0009-2541(87)90108-2.

Lear, C.H., Elderfield, H., Wilson, P.A., 2000. Cenozoic deep-sea temperatures and global ice volumes from Mg/Ca in benthic foraminiferal calcite. Science 287, 269–272.

Lear, C.H., Bailey, T.R., Pearson, P.N., Coxall, H.K., Rosenthal, Y., 2008. Cooling and ice growth across the Eocene-Oligocene transition. Geology 36, 251–254.

Leng, M.J., Marshall, J.D., 2004. Palaeoclimate interpretation of stable isotope data from lake sediment archives. Quat. Sci. Rev. 23, 811–831.

Li, X.Z., Liu, W.G., Xu, L.M., 2012. Carbon isotopes in surface-sediment carbonates of modern Lake Qinghai (Qinghai–Tibet Plateau): Implications for lake evolution in arid areas. Chem. Geol. 300-301, 88–96. https://doi.org/10.1016/j.chemgeo.2012.01.010.

Li, S., Xing, Y., Valdes, P.J., Huang, Y., Su, T., Farnsworth, A., Lunt, D.J., Tang, H., Kennedy, A.T., Zhou, Z., 2018. Oligocene climate signals and forcings in Eurasia revealed by plant macrofossil and modelling results. Gondwana Res. 61, 115–127. https://doi.org/10.1016/j.gr.2018.04.015.

Liu, Z., Pagani, M., Zinniker, D., DeConto, R., Huber, M., Brinkhuis, H., Shah, S.R., Leckie, R.M., Pearson, A., 2009. Global cooling during the Eocene-Oligocene climate transition. Science 323, 1187–1190.

Liu, W.G., Liu, Z.H., An, Z.S., Sun, J.M., Chang, H., Wang, N., Dong, J.B., Wang, H.Y., 2014. Late Miocene episodic lakes in the arid Tarim Basin, western China. Proc. Natl. Acad. Sci. U. S. A. 111, 16292–16296. https://doi.org/10.1073/pnas.1410890111.

Lü, L., Sun, J., Zhang, Z., Jia, Y., Tian, S., Abdulov, S., Gadoev, M., Oimahmadov, I., 2020. Late Miocene accelerated exhumation in the central Tajik Basin and implications for northward indention and lateral growth of the Pamir. Tectonophysics 787, 228438. https://doi.org/10.1016/j.tecto.2020.228438.

Meijer, N., Dupont-Nivet, G., Abels, H.A., Kaya, M.Y., Licht, A., Xiao, M., Zhang, Y., Roperch, P., Poujol, M., Lai, Z., Guo, Z., 2019. Central Asian moisture modulated by proto-Paratethys Sea incursions since the early Eocene. Earth Planet. Sci. Lett. 510, 73–84. https://doi.org/10.1016/j.epsl.2018.12.031.

Meng, J., McKenna, M.C., 1998. Faunal turnovers of Palaeogene mammals from the Mongolian Plateau. Nature 394, 364–367.

Miller, K.G., Fairbanks, R.G., 1985. Oligocene to Miocene carbon isotope cycles and abyssal circulation changes. In: Sundquist, E.T., Broecker, W.S. (Eds.), The Carbon Cycle and Atmospheric CO_2: Natural Variations Archean to Present, Geophys. Monogr. Ser., 32, pp. 469–486.

Miller, K.G., Janecek, T.R., Katz, M.E., Keil, D.J., 1987. Abyssal circulation and benthic foraminiferal changes near the Paleocene/Eocene boundary. Paleoceanography 2, 741–761.

Miller, K.G., Browning, J.V., Schmelz, W.J., Kopp, R.E., Mountain, G.S., Wright, J.D., 2020. Cenozoic sea-level and cryospheric evolution from deep-sea geochemical and continental margin records. Sci. Adv. 6 https://doi.org/10.1126/sciadv.aaz1346 eaaz1346.

Myrbo, A., Shapley, M.D., 2006. Seasonal water-column dynamics of dissolved inorganic carbon stable isotopic compositions ($\delta^{13}C$ DIC) in small hardwater lakes in Minnesota and Montana. Geochim. Cosmochim. Acta 70, 2699–2714.

Nesbitt, H.W., Young, G.M., 1982. Early Proterozoic climates and plate motions inferred from major element chemistry of lutites. Nature 299, 715–717.

Nesbitt, H.W., Young, G.M., 1984. Prediction of some weathering trends of plutonic and volcanic rocks based on thermodynamic and kinetic considerations. Geochim. Cosmochim. Acta 48, 1523–1534.

Nesbitt, H.W., Markovics, G., Price, R.C., 1980. Chemical processes affecting alkalis and alkalineearths during continental weathering. Geochim. Cosmochim. Acta 44, 1659–1666.

Pagani, M., Huber, M., Liu, Z.H., Bohaty, S., Henderiks, J., Sijp, W., Krishnan, S., DeConto, R., 2011. The role of carbon dioxide during the onset of Antarctic glaciation. Science 334, 1261–1264. https://doi.org/10.1126/science.1203909.

Page, M., Licht, M.A., Dupont-Nivet, G., Meijer, N., Guo, Z., 2019. Synchronous cooling and decline in monsoonal rainfall in northeastern Tibet during the fall into the Oligocene icehouse. Geology 47, 203–206. https://doi.org/10.1130/G45480.1.

Paprocka, A., 2007. Stable carbon and oxygen isotopes in recent sediments of Lake Wigry, NE Poland: implications for lake morphometry and environmental changes. Terrstr. Ecol. 1, 267–281.

Parker, A., 1970. An index of weathering for silicate rocks. Geol. Mag. 107, 501–504.

Popov, S.V., Rögl, F., Rozanov, A.Y., Steininger, F.F., Shcherba, I.G., Kovac, M., 2004. Lithological-paleogeographic maps of Paratethys 10 maps late Eocene to Pliocene. Cour. Forsch. -Inst. Senckenberg 250, 1–46.

Price, J.R., Velbel, M.A., 2003. Chemical weathering indices applied to weathering profiles developed on heterogeneous felsic metamorphic parent rocks. Chem. Geol. 202, 397–416.

Prud'homme, C., Scardia, G., Vonhof, H., Guinoiseau, D., Nigmatova, S., Fiebig, J., Gerdes, A., Janssen, R., Fitzsimmons, K.E., 2021. Central Asian modulation of Northern Hemisphere moisture transfer over the Late Cenozoic. Commun. Earth Environ. 2, 106. https://doi.org/10.1038/s43247-021-00173-z.

Qi, L., Hu, J., Gregoire, D.C., 2000. Determination of trace elements in granites by inductively coupled plasma mass spectrometry. Talanta 51, 507–513.

Ramstein, G., Fluteau, F., Besse, J., Joussaume, S., 1997. Effect of orogeny, plate motion and land–sea distribution on Eurasian climate change over the past 30 million years. Nature 386, 788–795.

Retallack, G.J., 1986. The fossil record of soils. In: Wright, V.P. (Ed.), Paleosols, Their Recognition and Interpretation. Blackwell, London, pp. 1–57.

Retallack, G.J., 1999. Post-apocalyptic greenhouse paleoclimate revealed by earliest Triassic paleosols in the Sydney Basin, Australia. Geol. Soc. Am. Bull. 111, 52–70.
Rögl, F., 1999. Mediterranean and Paratethys. Facts and hypotheses of an Oligocene to Miocene paleogeography (short overview). Geol. Carpath. 50, 339–349.
Rubatto, D., Hermann, J., 2001. Exhumation as fast as subduction? Geology 29, 3–6.
Rubatto, D., Gebauer, D., Fanning, M., 1998. Jurassic formation and Eocene subduction of the Zermatt–Saas–Fee ophiolites: implications for the geodynamic evolution of the Central and Western Alps. Contrib. Mineral. Petrol. 132, 269–287.
Schulz, H.M., Bechtel, A., Sachsenhofer, R.F., 2005. The birth of the Paratethys during the Early Oligocene: from Tethys to an ancient Black Sea analogue? Glob. Planet. Chang. 49, 163–176. https://doi.org/10.1016/j.gloplacha.2005.07.001.
Siegenthaler, U., Oeschger, H., 1980. Correlation of ^{18}O in precipitation with temperature and altitude. Nature 285, 314–317.
Sun, J.M., Windley, B.F., 2015. Onset of aridification by 34 Ma across the Eocene–Oligocene transition in Central Asia. Geology 43, 1015–1018. https://doi.org/10.1130/G37165.1.
Sun, J.M., Ni, X.J., Bi, S.D., Wu, W.Y., Ye, J., Meng, J., Windley, B.F., 2014. Synchronous turnover of flora, fauna, and climate at the Eocene–Oligocene boundary in Asia. Sci. Rep. 4, 7463. https://doi.org/10.1038/srep07463.
Sun, J.M., Windley, B.F., Zhang, Z.L., Fu, B.H., Li, S.H., 2016. Diachronous seawater retreat from the southwestern margin of the Tarim Basin in the late Eocene. J. Asian Earth Sci. 116, 222–231. https://doi.org/10.1016/j.jseaes.2015.11.020.
Sun, J., Liu, W., Liu, Z., Deng, T., Windley, B.F., Fu, B., 2017. Extreme aridification since the beginning of the Pliocene in the Tarim Basin, western China. Palaeogeogr. Palaeoclimatol. Palaeoecol. 485, 189–200. https://doi.org/10.1016/j.palaeo.2017.06.012.
Sun, Y.Y., Liu, J., Liang, Y., Ji, J.L., Liu, W.G., Aitchison, J.C., Sun, J.M., Lu, J.F., Song, B.W., Xu, Y.D., Zhang, K.X., Liu, Z.H., 2020a. Cenozoic moisture fluctuations on the northeastern Tibetan Plateau and association with global climatic conditions. J. Asian Earth Sci. 200, 104490. https://doi.org/10.1016/j.jseaes.2020.104490.
Sun, J.M., Zhang, Z.L., Cao, M.M., Windley, B.F., Tian, S.C., Sha, J.G., Abdulov, S., Gadoev, M., Oimahmadov, I., 2020b. Timing of seawater retreat from proto-Paratethys, sedimentary provenance, and tectonic rotations in the late Eocene-early Oligocene in the Tajik Basin, Central Asia. Palaeogeogr. Palaeoclimatol. Palaeoecol. 545, 109657. https://doi.org/10.1016/j.palaeo.2020.109657.
Talbot, M.R., 1990. A review of the palaeohydrological interpretation of carbon and oxygen isotopic ratios in primary lacustrine carbonates. Chem. Geol. 80, 261–279.
Talbot, M.R., Kelts, K., 1986. Primary and diagenetic carbonates in the anoxic sediments of Lake Bosumtwi, Ghana. Geology 14, 912–916.
Thomas, J.-C., Chauvin, A., Gapais, D., Bazhenov, M.L., Perroud, H., Cobbold, P.R., Buttman, V.S., 1994. Paleomagnetic evidence for Cenozoic block rotations in the Tadjik depression (Central Asia). J. Geophys. Res. 99, 15,141–15,160.
Vogel, D.E., 1975. Precambrian weathering in acid metavolcanic rocks from the Superior Province, Villebon Township, South–Central Quebec. Can. J. Earth Sci. 12, 2080–2085.
Vreča, P., 2003. Carbon cycling at the sediment-water interface in a eutrophic mountain lake (Jezero na Planini pri Jezeru, Slovenia). Org. Geochem. 34, 671–680.
Wang, X., Carrapa, B., Chapman, J.B., Henriquez, S., Wang, M., DeCelles, P.G., Li, Z.J., Wang, F., Oimuhammadzoda, I., Gadoev, M., Chen, F.H., 2019. Parathethys last gasp in Central Asia and Late Oligocene accelerated uplift of the Pamirs. Geophys. Res. Lett. 46, 11,773–11,781. https://doi.org/10.1029/2019GL084838.
Wang, X., Carrapa, B., Sun, Y., Dettman, D.L., Chapman, J.B., Caves Rugenstein, J.K., Clementz, M.T., DeCelles, P.G., Wang, M., Chen, J., Quade, J., Wang, F., Li, Z., Oimuhammadzoda, I., Gadoev, M., Lohmann, G., Zhang, X., Chen, F., 2020. The role of the westerlies and orography in Asian hydroclimate since the late Oligocene. Geology 48, 728–732. https://doi.org/10.1130/G47400.1.
Xiao, G.Q., Abels, H.A., Yao, Z.Q., Dupont-Nivet, G., Hilgen, F.J., 2010. Asian aridification linked to the first step of the Eocene–Oligocene climate transition (EOT) in obliquity-dominated terrestrial records (Xining Basin, China). Clim. Past 6, 501–513.
Ye, C.C., Yang, Y.B., Fang, X.M., Hong, H.L., Wang, C.W., Yang, R.S., Zhang, W.L., 2018. Chlorite chemical composition change in response to the Eocene-Oligocene climate transition on the northeastern Tibetan Plateau. Palaeogeogr. Palaeoclimatol. Palaeoecol. 512, 23–32. https://doi.org/10.1016/j.palaeo.2018.03.014.
Zachos, J., Pagani, M., Sloan, L., Thomas, E., Billups, K., 2001. Trends, rhythms, and aberrations in global climate 65 Ma to present. Science 292, 686–693.
Zachos, J.C., Dickens, G.R., Zeebe, R.E., 2008. An early Cenozoic perspective on greenhouse warming and carbon-cycle dynamics. Nature 451, 279–283.
Zakharov, S.A., 1962. Tectonic provinces and structural map of Tadjikian depression. Trans. Geol. Acad. Sci. Tadjikistan Repub. 5.
Zhang, C.X., Guo, Z.T., 2014. Clay mineral changes across the Eocene–Oligocene transition in the sedimentary sequence at Xining occurred prior to global cooling. Palaeogeogr. Palaeoclimatol. Palaeoecol. 411, 18–29.
Zhang, Z., Wang, H., Guo, Z., Jiang, D., 2007. What triggers the transition of palaeoenvironmental patterns in China, the Tibetan Plateau uplift or the Paratethys Sea retreat? Palaeogeogr. Palaeoclimatol. Palaeoecol. 245, 317–331.
Zhang, R., Jiang, D., Zhang, Z., Zhang, C., 2021. Effects of Tibetan Plateau growth, Paratethys Sea retreat and global cooling on the East Asian climate by the early Miocene. Geochem. Geophys. Geosyst. 22 https://doi.org/10.1029/2021GC009655 e2021GC009655.